NASA TECHNICAL MEMORANDUM

NASA TM X-3006

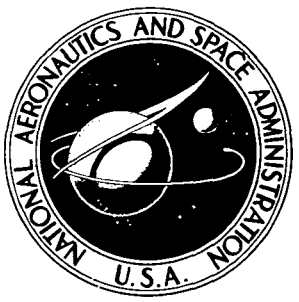

NASA TM X-3006

COLD-AIR ANNULAR-CASCADE INVESTIGATION OF AERODYNAMIC PERFORMANCE OF COOLED TURBINE VANES

I - Facility Description and Base (Solid) Vane Performance

by Louis J. Goldman and Kerry L. McLallin

Lewis Research Center
Cleveland, Ohio 44135

NATIONAL AERONAUTICS AND SPACE ADMINISTRATION • WASHINGTON, D. C. • MARCH 1974

1. Report No.	2. Government Accession No.	3. Recipient's Catalog No.
NASA TM X-3006		

4. Title and Subtitle	5. Report Date
COLD-AIR ANNULAR-CASCADE INVESTIGATION OF AERODYNAMIC PERFORMANCE OF COOLED TURBINE VANES. I - FACILITY DESCRIPTION AND BASE (SOLID) VANE PERFORMANCE	March 1974
	6. Performing Organization Code

7. Author(s)	8. Performing Organization Report No.
Louis J. Goldman and Kerry L. McLallin	E-7699
	10. Work Unit No. 501-24

9. Performing Organization Name and Address	11. Contract or Grant No.
Lewis Research Center National Aeronautics and Space Administration Cleveland, Ohio 44135	

12. Sponsoring Agency Name and Address	13. Type of Report and Period Covered
National Aeronautics and Space Administration Washington, D.C. 20546	Technical Memorandum
	14. Sponsoring Agency Code

15. Supplementary Notes

16. Abstract

The aerodynamic performance of a solid vane was experimentally determined in a full-annular cascade, where three-dimensional effects could be obtained. This vane was of the same size and profile as the cooled vanes to be subsequently tested. The vanes were tested over a pressure ratio range that corresponded to mean-radius ideal aftermixed critical velocity ratios of 0.71 to 0.89. Overall vane aftermixed efficiencies were obtained over this range of critical velocity ratios and compared with results from a four-vane annular-sector cascade. The variation in vane aftermixed conditions and vane aftermixed efficiency with radius were also obtained and compared with design values. Vane surface static-pressure distributions were measured and compared with theory and with the results obtained in the four-vane cascade.

17. Key Words (Suggested by Author(s))	18. Distribution Statement
Aerodynamic performance Annular cascade Turbine cooling Cooled vanes	Unclassified - unlimited Cat. 01

19. Security Classif. (of this report)	20. Security Classif. (of this page)	21. No. of Pages	22. Price*
Unclassified	Unclassified	30	$3.00

* For sale by the National Technical Information Service, Springfield, Virginia 22151

COLD-AIR ANNULAR-CASCADE INVESTIGATION OF AERODYNAMIC PERFORMANCE OF COOLED TURBINE VANES

I - FACILITY DESCRIPTION AND BASE (SOLID) VANE PERFORMANCE

by Louis J. Goldman and Kerry L. McLallin

Lewis Research Center

SUMMARY

The aerodynamic performance of a solid vane was experimentally determined in a full-annular cascade, where three-dimensional effects could be obtained. This vane was of the same size and profile as the cooled vanes to be subsequently tested. The vanes were tested over a pressure ratio range that corresponded to mean-radius ideal aftermixed critical velocity ratios of 0.71 to 0.89. Overall vane aftermixed efficiencies were obtained over this range of critical velocity ratios and compared with results from a four-vane annular-sector cascade. The variation in vane aftermixed conditions and vane aftermixed efficiency with radius were also obtained and compared with design values. Vane surface static-pressure distributions were measured and compared with theory and with the results obtained in the four-vane cascade.

In general, the experimental vane surface pressure distributions obtained in the full-annular cascade agree well with those from the four-vane cascade and with theoretical results obtained for the guided portion of the passage. The largest deviations in aftermixed flow angle and in aftermixed static-pressure ratio from the design values were in the hub region. These large deviations were caused, in part, by probe blockage, which is largest at the hub and tends to decrease the flow locally. The vane efficiency decreased rapidly near the hub and tip walls, with the maximum value not occurring at the mean radius. The overall efficiency was fairly constant at 0.957 over the critical velocity ratio range investigated and agreed well with the results obtained in the four-vane cascade.

INTRODUCTION

The requirement for cooling the turbine vanes and blades of high-temperature air-

craft engines has resulted in a program of turbine cooling studies being conducted at the Lewis Research Center. One part of this program is the study of the aerodynamic performance of vanes with different cooling schemes. Performance results for cooled turbine vanes studied in a four-vane annular-sector cascade are reported in references 1 and 2. Reference 1 presents the total-pressure distribution at the vane exit and the vane surface static-pressure distribution at three radial sections for the base (solid) vane. Reference 2 presents the aerodynamic performance of the solid vane, as well as the performance of a convection-film-cooled vane and a transpiration-cooled vane at gas-coolant temperature ratios to 2.75. These annular-sector results are somewhat limited in value because true three-dimensional gradients could not be adequately simulated in the four-vane cascade.

An investigation was, therefore, undertaken wherein the previously mentioned turbine vanes, among others, would be studied in a full-annular cascade, where valid three-dimensional effects could be obtained. The cascade was designed for cold-air studies primarily at a gas-coolant temperature ratio of 1. The first phase of the study was to obtain the aerodynamic performance of the solid vanes so that a comparison with the results from the four-vane cascade could be made. Subsequent studies would then determine the performance of the different cooling configurations for comparison with both the solid full-annular results and the results from the four-vane cascade.

This report describes the full-annular cascade and presents the experimental results for the solid vane. The solid vane was tested over a pressure ratio range that corresponded to mean-radius ideal aftermixed critical velocity ratios of 0.71 to 0.89. Overall vane efficiencies were obtained over this range of critical velocity ratios and compared with the four-vane-cascade results. The variation in vane aftermixed conditions and in aftermixed efficiency with radius are also presented. In addition, vane surface static-pressure measurements were obtained and compared with theory and with measurements obtained in the four-vane cascade.

APPARATUS AND PROCEDURE

Cascade Facility

The full-annular cascade facility consists essentially of an inlet section, a test section, and an exit section. The actual facility and a schematic cross-sectional view of the facility are shown in figures 1 and 2, respectively. In operation, room-temperature air is drawn through the inlet section, the blading, and the exit section and then exhausted through the laboratory altitude exhaust system.

Inlet section. - The inlet, consisting of a bellmouth and a short straight section,

Figure 1. - 81-Centimeter-diameter (32-in.) full-annular cascade.

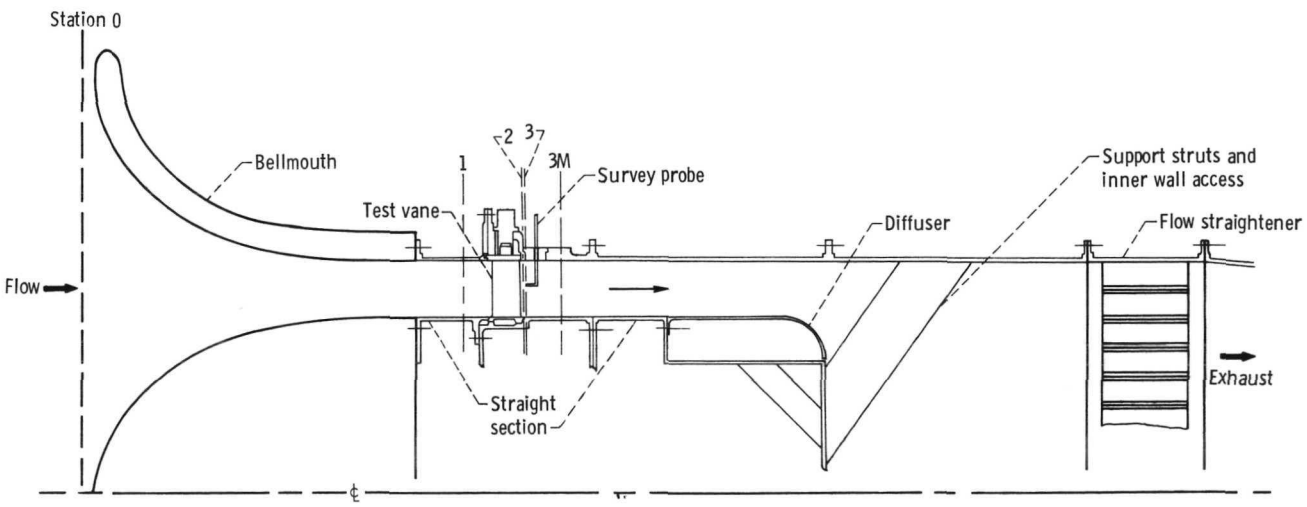

Figure 2. - Schematic cross-sectional view of 81-centimeter-diameter (32-in.) full-annular cascade.

was designed to accelerate the flow to uniform parallel conditions at the vane inlet. The bellmouth profile was designed to provide a smooth transition to the straight section.

Test section. - The test section consists of a sector of five vanes which are part of the full-annular ring of 72 vanes. The annulus has an inner diameter of 61.48 centimeters (24.21 in.) and an outer diameter of 81.03 centimeters (31.90 in.). For the solid-vane investigation, all 72 vanes were identical. For subsequent investigations, the five test vanes will be replaced with cooled vanes having the same aerodynamic profile as the solid vanes.

The coordinates of the solid-vane profile are given in references 1 and 2. The twisted vane has a height of 9.78 centimeters (3.85 in.), an axial chord of 5.08 centimeters (2.00 in.) at the mean radius, and an axial solidity of 1.64 at the mean radius. A schematic of the vane profiles at the hub, mean, and tip radii is shown in figure 3.

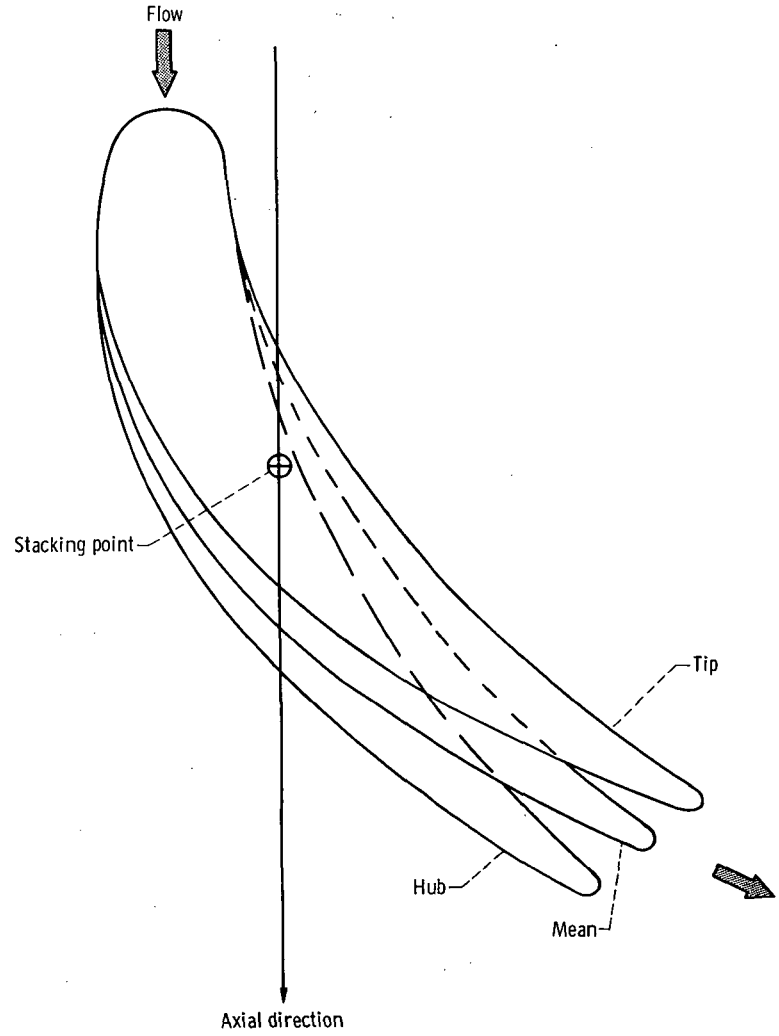

Figure 3. - Schematic of vane profile.

Exit section. - The exit section consists primarily of a diffusing section and a flow-straightening section. The diffusing section was designed to decelerate the flow gradually downstream of the test section. Because of mechanical failure, the diffuser was removed for this investigation. This removal resulted in a more rapid deceleration of the flow but did not seem to affect cascade operation adversely. The flow straightener was designed to turn the swirling flow back to the axial direction prior to its entering the laboratory exhaust system. The straightener consists of a bundle of short tubes with centerlines parallel to the axis of the cascade (fig. 2).

Instrumentation

Instrumentation was provided primarily to measure static wall pressures at various locations, vane surface static pressures at different radii, and survey data of total pressure, total temperature, static pressure, and flow angle downstream of the test vanes. Figure 2 shows the station nomenclature used for the instrumentation.

Total conditions. - Total temperature and pressure were measured at the cascade inlet (station 0). The total temperature of the entering air was measured by four copper-constantan thermocouples located 90° apart circumferentially at the bellmouth inlet. The ambient total pressure was measured by a barometer. It was assumed that no loss of total pressure or temperature occurred between station 0 and station 1 (vane inlet).

Wall static pressures. - Static pressures were measured by taps located on both the inner (hub) and outer (tip) walls of the cascade. At the vane inlet (station 1), four taps were located 90° apart circumferentially. These static pressures were used to ascertain the uniformity of the flow entering the vanes as well as to provide information for estimates of the incoming airflow rate. At the vane exit (stations 2 and 3), taps were located along the mean streamlines of each of the test vanes as shown in figure 4. In addition, four taps were located at station 3, spanning the center test vane. These pressures were used to indicate the uniformity of the flow in the test section. Static taps were also located far downstream of the vanes where we believed the flow would be mixed to relatively uniform conditions (station 3M). These pressures were used to set the flow conditions in the cascade.

Vane surface static pressures. - Two of the test vanes were instrumented with a total of 42 surface static-pressure taps as shown in figure 5. One vane was instrumented with 20 taps located at the mean radius. The second vane had 22 taps which were divided equally between sections located 1.59 centimeters (5/8 in.) from the vane hub and tip platforms. As figure 5 shows, the pressure tubing was installed in grooves machined into the vane surface. After the tubing was installed, the grooves were filled

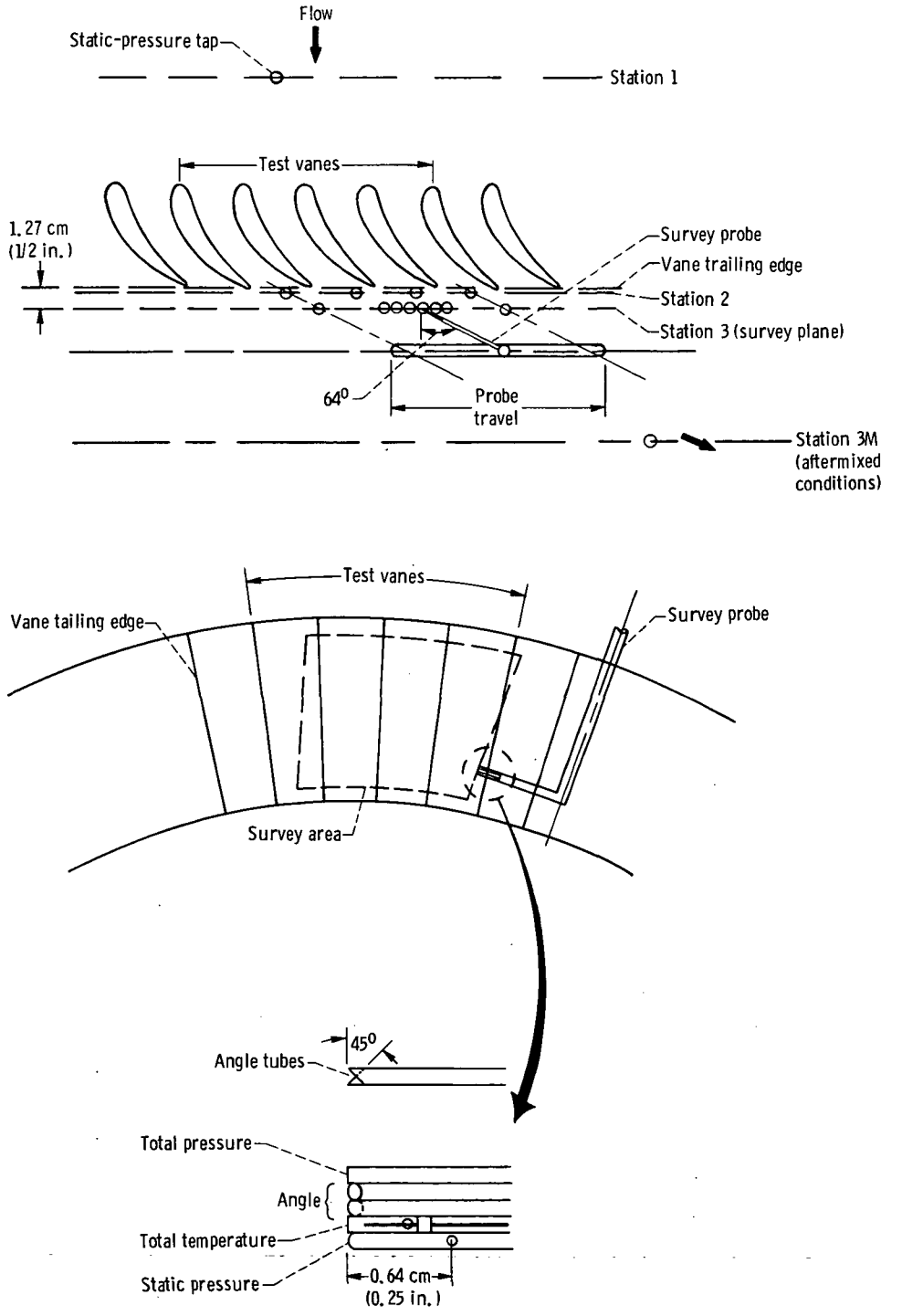

Figure 4. - Schematic of instrumentation for survey data.

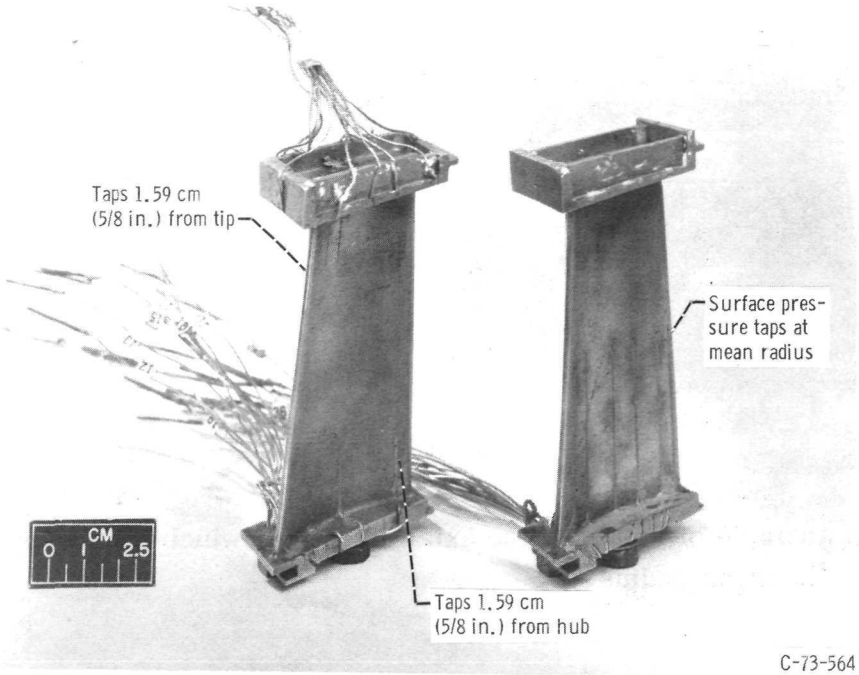

Figure 5. - Instrumented solid vanes.

and faired to the contour of the vane surface. The static-pressure taps were 0.051 centimeter (0.020 in.) in diameter.

Survey probe. - A calibrated probe was located downstream of the test vanes (fig. 4). The survey plane (station 3) was 1.27 centimeters (1/2 in.) downstream of the vane trailing edge in the axial direction. The probe was capable of motion in both the radial and circumferential directions. As figure 4 shows, the probe could travel circumferentially over the middle three of the five test vanes. The radial position of the probe was limited, in general, to the survey area shown in figure 4. This limitation was necessary because of the large boundary-layer buildup on the end walls (possibly caused by the large wooden bellmouth inlet) and the fact that the probe geometry restricted radial motion near the walls.

The calibrated combination probe used for the survey measured total pressure, total temperature, static pressure, and flow angle. The probe is shown in figure 6. The probe tip was made of stainless-steel tubing with outside diameter of 0.102 centimeter (0.040 in.) and a wall thickness of 0.018 centimeter (0.007 in.).

The loss in total pressure was obtained from a total head tube with an inside bevel of 30°. Static pressure was measured by using a Prandtl tube. The flow angle was determined from the measured pressure difference of two 45°-angled tubes (fig. 4). All pressures were measured with calibrated strain-gage pressure transducers. The total temperature was obtained from a Chromel-Alumel aspirated thermocouple. The probe

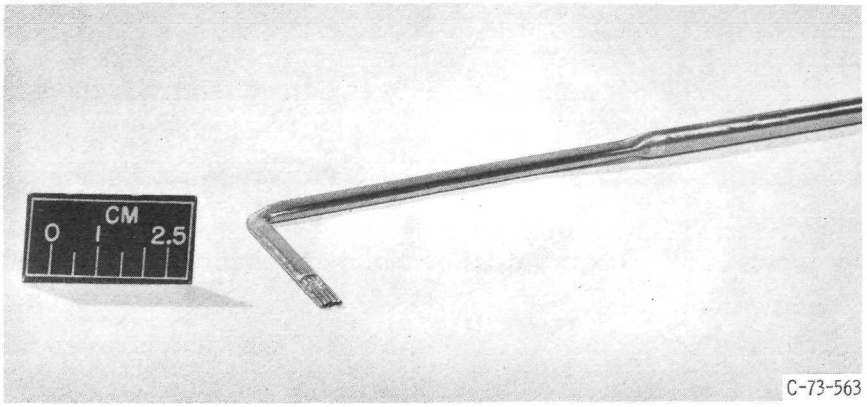

Figure 6. - Survey probe.

was positioned at an angle of 64° from the axial direction, which corresponds to the design flow angle at the mean radius.

Procedure

Atmospheric air from the test cell was drawn through the cascade and exhausted into the laboratory altitude exhaust system. Test conditions were set by controlling the pressure ratio across the blade row with two throttle valves located in the exhaust system. Static taps located downstream of the test section where the flow was assumed to be circumferentially uniform (station 3M) were used to set this pressure ratio.

The solid vanes were tested over a pressure ratio range that corresponded to mean-radius ideal aftermixed critical velocity ratios of 0.71 to 0.89. The design value for the vanes is 0.87. At a given pressure ratio, probe survey data were obtained at a number of different radii over the blade height. At any fixed radius, the probe was moved circumferentially over three vane passages with survey data being obtained continuously. The slow speed of the circumferential drive motor resulted in survey data (total pressure, total temperature, static pressure, flow angle, and circumferential position) being obtained at approximately 0.04° increments. The spacing Θ between vanes in the annular cascade is 5°. (All symbols are defined in appendix A.) The output signals of the thermocouple and pressure transducers were digitized and recorded on magnetic tape.

Data Reduction

The solid vane performance presented herein was calculated from the exit survey measurements of total pressure, total temperature, static pressure, flow angle, and probe position. Data from the middle wake (of the three wakes that were measured) were used in these calculations.

As described in appendix B, conservation of mass, momentum, and energy is applied to an annular-sector control volume to obtain an aftermixed state (station 3M) where the flow is considered circumferentially uniform. The vane efficiency obtained for the aftermixed state contains not only the profile loss, but also the mixing loss. The sum of the losses is, however, theoretically independent of the axial location of the survey measurement plane. For solid vanes, the vane aftermixed efficiency based on kinetic energy can be defined as a function of radius $\overline{\eta}_{3M}(r)$ or as an overall quantity $\overline{\overline{\eta}}_{3M}$, as given by the following equations from appendix B:

$$\overline{\eta}_{3M}(r) = \frac{V_{3M}^2(r)}{V_{3M,\,id}^2(r)} \tag{B29}$$

$$\overline{\overline{\eta}}_{3M} = \frac{\int_{r_i}^{r_o} \rho_{3M}(r) V_{3M,\,z}(r) V_{3M}^2(r) r\, dr}{\int_{r_i}^{r_o} \rho_{3M}(r) V_{3M,\,z}(r) V_{3M,\,id}^2(r) r\, dr} \tag{B30}$$

where

$$V_{3M,\,id}(r) = \sqrt{\left(\frac{2\gamma}{\gamma - 1}\right) g R T_0' \left\{1 - \left[\frac{p_{3M}(r)}{p_0'}\right]^{\frac{\gamma-1}{\gamma}}\right\}} \tag{B31}$$

The total-pressure-loss coefficient as a function of radius $\overline{\omega}_{3M}(r)$ can be defined by

$$\overline{\omega}_{3M}(r) = \frac{p_0' - p_{3M}'(r)}{p_0' - p_{3M}(r)} \tag{B32}$$

The method of obtaining the aftermixed conditions (i.e., $V_{3M}(r)$, $p_{3M}(r)$, etc.) from the survey measurements is described in appendix B. In the preceding equations, it has been assumed that the total pressure and temperature at the vane inlet (station 1) are equal to the total pressure and temperature at the cascade inlet (station 0).

RESULTS AND DISCUSSION

Effect of Probe Blockage on Flow Conditions

The survey probe, because of its physical presence, tends to influence the flow conditions locally around the probe. As figure 6 shows, the probe stem was made as thin as mechanical integrity would allow so that this effect would be minimized. The effect of the probe on the wall static pressures at the measuring location (station 3) is shown in figure 7. Wall taps at the hub and tip were located as shown in the figure. The blockage was found to be a function of both the circumferential position of the probe and its radial position. The data shown in figure 7 are for the probe in the center vane's wake, where it has the largest effect on the taps around the center vane. The pressure ratio p_{3M}/p_0' was held constant for these tests while data were taken with the probe at the hub, mean, and tip radii. For comparison, the probe was removed and the results are indicated by the solid lines. The probe blockage tends to decrease the flow locally, with a resultant increase in the static pressure. The effect is more pronounced

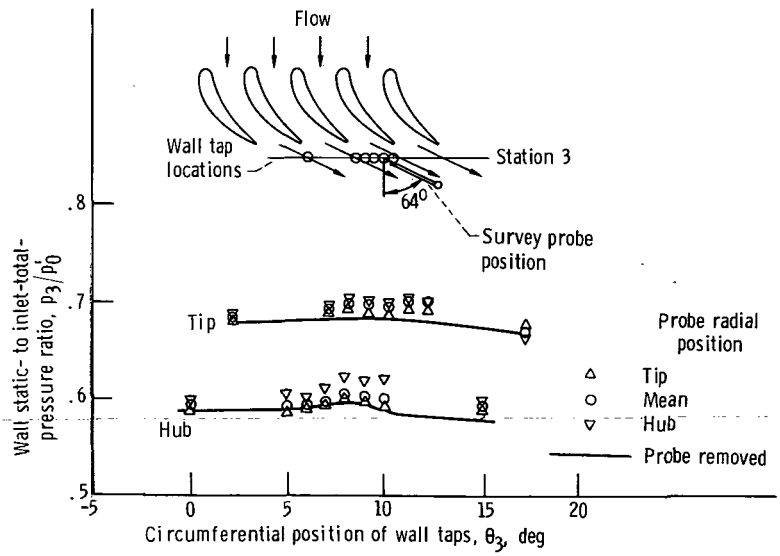

Figure 7. - Effect of survey probe blockage on wall static-pressure readings (probe in middle test vane wake).

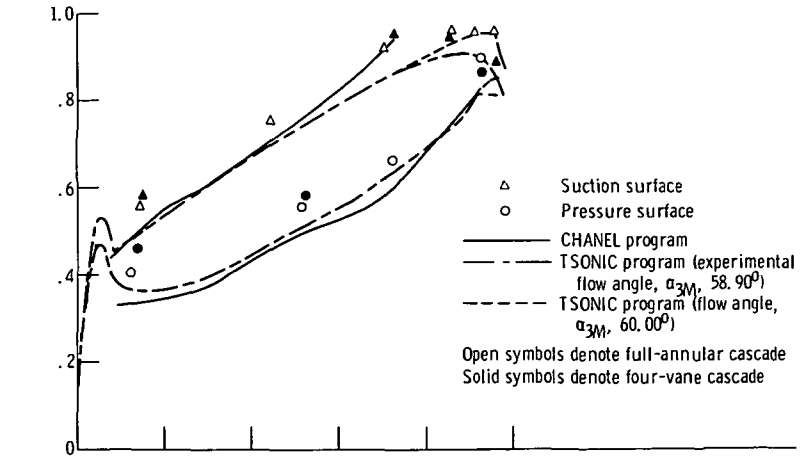

(a) Hub radius.

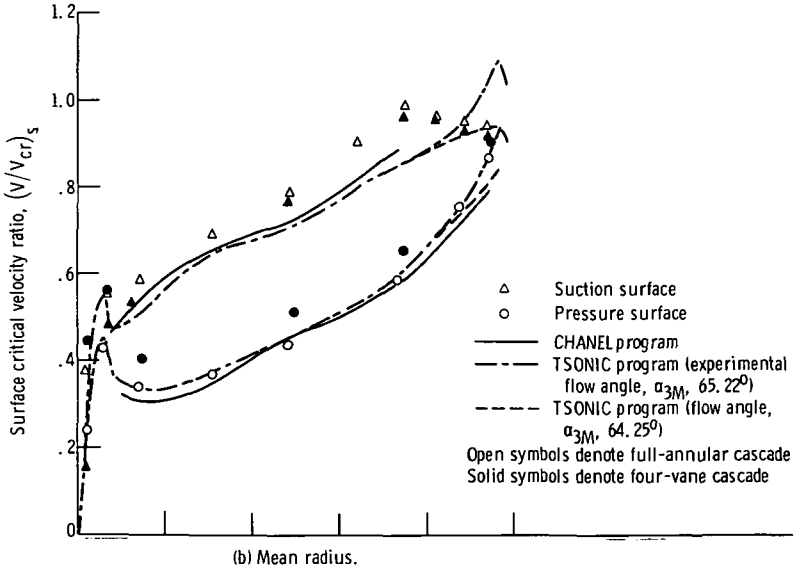

(b) Mean radius.

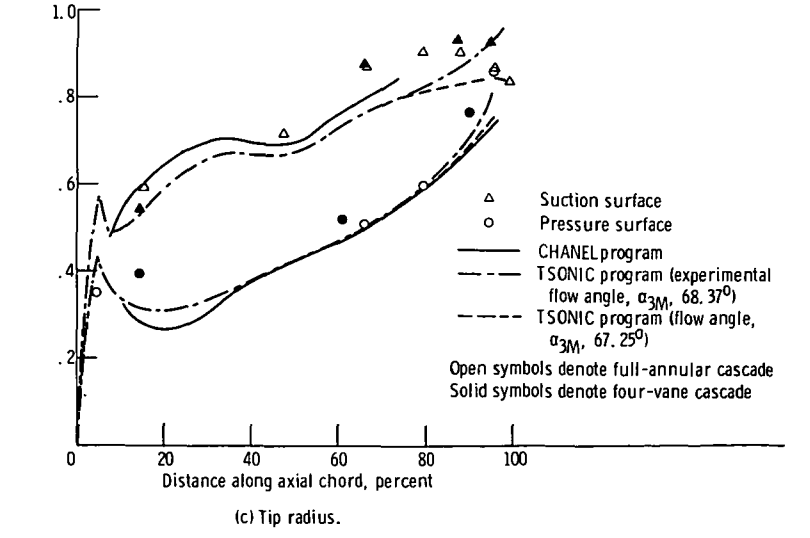

(c) Tip radius.

Figure 8. - Distribution of vane surface critical velocity ratio at $(V_{3M}/V_{cr,3M})_{id,mean} = 0.862$.

with the probe at the hub radius since the blockage is the largest at this location. Because the vane efficiency does not vary significantly with static- to total-pressure ratio (ref. 2), the probe blockage reported herein should have a negligible effect on the measured efficiency.

Vane Surface Critical Velocity Ratio Distributions

The vane surface critical velocity ratio distributions measured at the hub, mean, and tip radii are presented in figure 8. The surface distributions are compared with those obtained in the four-vane annular-sector cascade (ref. 1), as well as with theoretical results. The theoretical calculations were obtained from the computer programs CHANEL and TSONIC, described in references 3 and 4, respectively. The CHANEL program is for quasi-three-dimensional flow but is limited to the guided portion of the passage. The TSONIC program calculates the flow conditions for the entire passage but is limited to two-dimensional flow. The radial variation of stream sheet thickness, which is needed as input for TSONIC, was obtained from the CHANEL results. Using the experimentally determined exit conditions (weight flow and flow angle) as input for TSONIC resulted in choked conditions (large velocity peaks in figs. 8(b) and (c)) in the unguided portion of the passage for the mean and tip radii. Experimentation with the program indicated that the TSONIC results in this region were sensitive to the exit flow angle. Decreases of around 1° in the exit flow angle at the mean and tip were found to be needed to prevent choking. This magnitude of change in flow angle is probably within the accuracy of the measurement. Agreement between the experimental results and the theoretical (TSONIC and CHANEL) results was good for the guided portion of the passage. In general, the agreement between the experimental results for the full-annular and four-vane cascades was also good.

Aftermixed Conditions and Vane Performance

Typical exit survey data taken at the mean radius, near design conditions, are shown in figure 9. The exit measurements are essentially periodic over the total survey travel. In general, the wakes were essentially periodic for all radial surveys except near the hub and tip walls.

As explained in the section Data Reduction, these survey measurements were used to find the aftermixed conditions at each radius where survey data were taken. The aftermixed flow angle α_{3M} and the aftermixed static- to inlet-total-pressure ratio p_{3M}/p'_0 varied with radius at near design mean-radius ideal aftermixed critical velocity

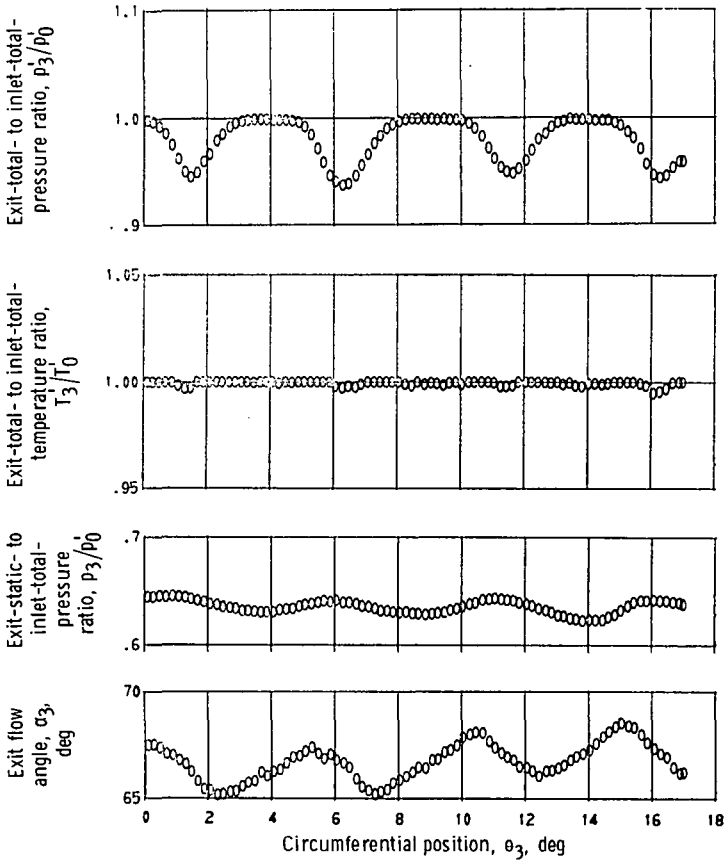

Figure 9. - Circumferential variation of survey measurements at mean radius.

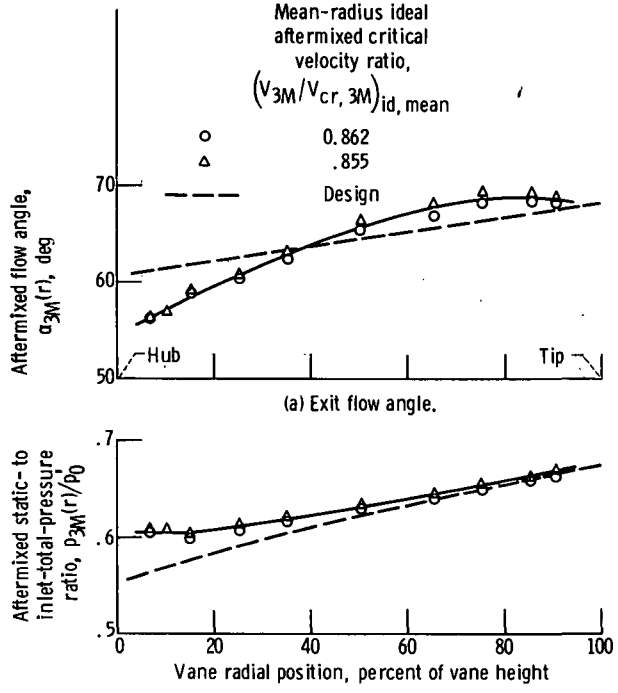

Figure 10. - Radial variation of exit flow angle and static- to total-pressure ratio.

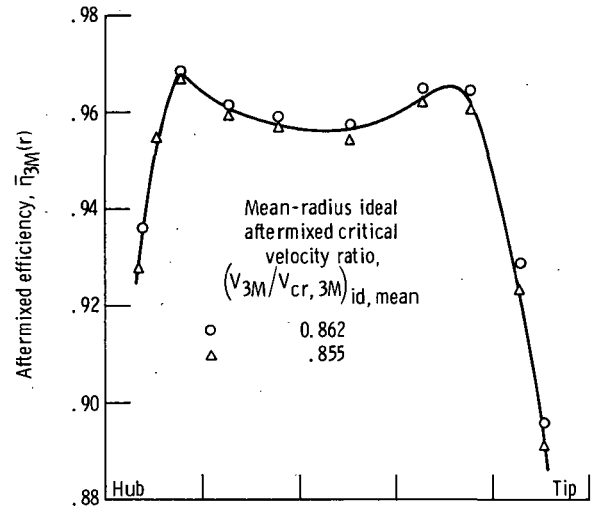

(a) Efficiency.

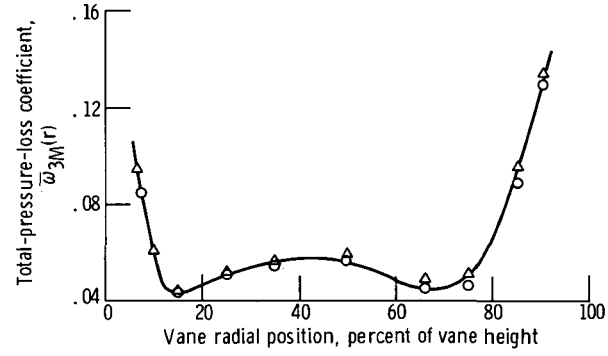

(b) Total-pressure-loss coefficient.

Figure 11. - Radial variation of efficiency and total-pressure-loss coefficient.

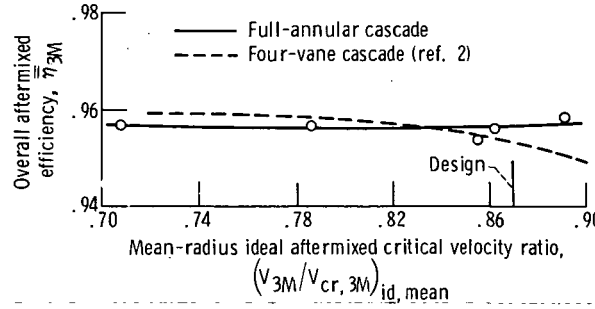

Figure 12. - Overall efficiency variation with ideal aftermixed critical velocity ratio at mean radius.

ratios as shown in figure 10. For comparison, the design values (indicated by dashed line) are also shown in the figure. The aftermixed conditions had the largest deviations from the design values in the hub region. These large deviations were caused, to some extent, by the probe blockage effects discussed previously.

The aftermixed efficiency $\bar{\eta}_{3M}(r)$ and total-pressure-loss coefficient $\bar{\omega}_{3M}(r)$ varied with radius at near-design mean-radius ideal aftermixed critical velocity ratios as shown in figures 11(a) and (b), respectively. As expected, the efficiency decreased rapidly near the walls because of the large losses associated with the end-wall boundary layers. These large losses near the walls are reflected as increased total-pressure-loss coefficients in figure 11(b). Interestingly, the efficiency was not highest at the mean radius. This may be caused partly by the secondary flow patterns established in the full-annular cascade, similar to those found in reference 5.

The overall aftermixed efficiency $\bar{\bar{\eta}}_{3M}$ varied with the aftermixed ideal critical velocity ratio at the mean radius as shown in figure 12. The efficiency was fairly constant at a value of 0.957 over the range investigated. The results of the four-vane cascade agreed well with those of the full-annular cascade.

SUMMARY OF RESULTS

The aerodynamic performance of a solid vane was experimentally determined in a full-annular cascade, where three-dimensional effects could be obtained. The vanes were tested over a pressure ratio range that corresponded to mean-radius ideal aftermixed critical velocity ratios of 0.71 to 0.89. Overall vane aftermixed efficiencies were obtained over this critical velocity ratio range and compared with results from a four-vane annular-sector cascade. The variation in vane aftermixed conditions and vane aftermixed efficiency with radius was also obtained and compared with design values. Vane surface static-pressure distributions were measured and compared with theory and with the results obtained in the four-vane cascade. The results of the investigation are summarized as follows:

1. The experimentally determined vane surface critical velocity ratio distribution agreed well with the theoretical results for the guided portion of the passage. In general, the agreement between the vane surface distributions obtained in the full-annular cascade and in the four-vane cascade was good.

2. The largest deviations in the aftermixed flow angle and in the aftermixed static- to inlet-total-pressure ratio from the design values were in the hub region. These large deviations are probably caused, in part, by probe blockage, which is largest at the hub and tends to decrease the flow locally.

3. The aftermixed efficiency decreased rapidly near the hub and tip walls because

of the large losses associated with the end-wall boundary layers. The efficiency was not the highest at the mean radius, possibly because of secondary flows being formed in the full-annular cascade.

4. The overall aftermixed efficiency was fairly constant at a value of 0.957 over the range investigated and agreed well with the values obtained in the four-vane cascade.

Lewis Research Center,
National Aeronautics and Space Administration,
Cleveland, Ohio, November 6, 1973,
501-24.

APPENDIX A

SYMBOLS

C_p	specific heat at constant pressure, J/kg-K (ft-lbf/lbm-^{o}R)
E	energy parameter, eq. (B15)
g	force-mass conversion constant, 32.174 lbm-ft/lbf-sec^2
J	mechanical equivalent of heat, 778.0 ft-lbf/Btu
J_z	axial momentum parameter, eq. (B13)
J_θ	tangential momentum parameter, eq. (B14)
M	Mach number
$\overline{m}$	mass flow parameter at radius r, eq. (B12)
$\overline{\overline{m}}$	total mass flow per passage, kg/sec (lbm/sec)
p	pressure, N/m^2 (lbf/ft^2)
R	gas constant, J/kg-K (ft-lbf/lbm-^{o}R)
r	radial direction, m (ft)
s	vane spacing, m (ft)
T	temperature, K (^{o}R)
u	coordinate in tangential direction for two-dimensional flow, m (ft)
V	velocity, m/sec (ft/sec)
y	mass flow fraction
z	axial direction, m (ft)
α	flow angle measured from axial direction, rad (deg)
γ	ratio of specific heats
η	local efficiency based on kinetic energy
$\overline{\eta}$	efficiency at radius r based on kinetic energy
$\overline{\overline{\eta}}$	overall efficiency based on kinetic energy
Θ	vane angular spacing, rad (deg)
θ	circumferential direction, rad (deg)
ρ	density, kg/m^3 (lbm/ft^3)

$\overline{\omega}$ total-pressure-loss coefficient at radius r

Subscripts:

c coolant flow

cr flow condition at Mach 1

h hub

i survey position closest to inner (hub) wall

id ideal or isentropic process

mean mean radius

o survey position closest to outer (tip) wall

p primary flow

s vane surface

T thermodynamic

t tip

z axial direction

θ tangential direction

0 station at inlet plane of cascade bellmouth, fig. 2

1 station at vane inlet, fig. 2

2 station downstream of vane trailing edge, fig. 2

3 station downstream of vane trailing edge where survey measurements were taken, fig. 2

3M station far downstream of vane trailing edge where flow is assumed to be circumferentially mixed (uniform), fig. 2

Superscript:

total-state condition

APPENDIX B

DETERMINATION OF THREE-DIMENSIONAL LOSS CHARACTERISTICS OF STATOR VANES FROM SURVEY MEASUREMENTS

Three-dimensional losses for stator vanes tested in annular cascades can be determined from surveys taken downstream of the vane trailing edge. Surveys must be obtained both circumferentially and radially for at least one vane passage. Generally, the probe is moved circumferentially at a number of fixed radii between the hub and tip walls. A calibrated probe capable of measuring the total pressure, static pressure, total temperature, and flow angle is used for the surveys. The probe position both radially and circumferentially must also be measured.

Because the flow in the annular cascade is confined by cylindrical inner and outer walls, it will be assumed that the stream surfaces downstream of the vanes are cylindrical. Thus, the radial component of velocity must be zero. The flow conditions, and the nomenclature used in the following discussion, are shown in figure 13. The symbols are defined in appendix A.

From the probe measurements at the survey plane (station 3), the velocity $V_3(r, \theta)$, the static temperature $T_3(r, \theta)$, and the density $\rho_3(r, \theta)$ are obtained from standard

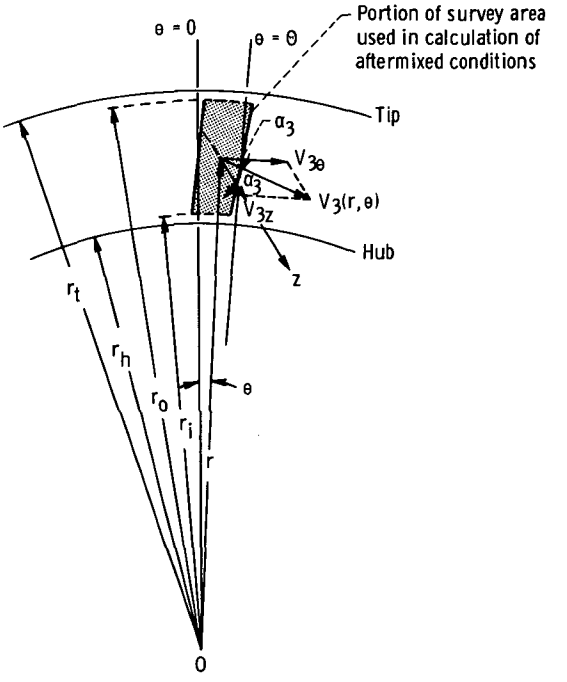

Figure 13. - Nomenclature at survey location (station 3).

isentropic flow relations. The uncooled vane efficiencies based on kinetic energy can be defined locally $\eta_3(r,\theta)$, at a given radius $\bar{\eta}_3(r)$, or overall $\bar{\bar{\eta}}_3$ by the following equations:

$$\eta_3(r,\theta) = \frac{\frac{1}{2}\rho_3(r,\theta)V_{3,z}(r,\theta)V_3^2(r,\theta)}{\frac{1}{2}\rho_3(r,\theta)V_{3,z}(r,\theta)V_{3,id}^2(r,\theta)} = \frac{V_3^2(r,\theta)}{V_{3,id}^2(r,\theta)} \tag{B1}$$

$$\bar{\eta}_3(r) = \frac{\int_0^{\Theta}\rho_3(r,\theta)V_{3,z}(r,\theta)V_3^2(r,\theta)r\,d\theta}{\int_0^{\Theta}\rho_3(r,\theta)V_{3,z}(r,\theta)V_{3,id}^2(r,\theta)r\,d\theta} \tag{B2}$$

$$\bar{\bar{\eta}}_3 = \frac{\int_{r_i}^{r_o}\int_0^{\Theta}\rho_3(r,\theta)V_{3,z}(r,\theta)V_3^2(r,\theta)r\,d\theta\,dr}{\int_{r_i}^{r_o}\int_0^{\Theta}\rho_3(r,\theta)V_{3,z}(r,\theta)V_{3,id}^2(r,\theta)r\,d\theta\,dr} \tag{B3}$$

where the ideal velocity $V_{3,id}(r,\theta)$ based on the vane inlet total pressure p_1' is

$$V_{3,id}(r,\theta) = \sqrt{\left(\frac{2\gamma}{\gamma-1}\right)gRT_1'\left\{1-\left[\frac{p_3(r,\theta)}{p_1'}\right]^{\frac{\gamma-1}{\gamma}}\right\}} \tag{B4}$$

From the geometry shown in figure 13, the axial velocity $V_{3,z}(r,\theta)$ is given by

$$V_{3,z}(r,\theta) = V_3(r,\theta)\cos\alpha_3(r,\theta) \tag{B5}$$

where $\alpha_3(r,\theta)$ is the flow angle measured from the axial direction. The θ-integration in equations (B2) and (B3) is from free stream to free stream over one vane spacing Θ. And the radial integrations are from the survey radius closest to the inner wall r_i to the survey radius closest to the outer wall r_o.

The efficiencies obtained in this manner, however, contain both the vane profile losses and losses due to mixing that occur downstream of the vane because of viscous effects and turbulent mixing. Since the mixing losses depend on the axial location of the

measuring plane, the efficiencies obtained from equations (B1) to (B3) will also depend on the axial location. Therefore, efficiencies obtained for vanes with different measuring station locations are not readily comparable. A solution to this shortcoming is to base the efficiency definition on a hypothetical state, where it is assumed that the flow has mixed to uniform conditions. This so-called aftermixed efficiency is then theoretically independent of the location of the measuring station.

The calculation procedure needed to obtain the aftermixed state for two-dimensional flow using boundary-layer parameters is described by Stewart in reference 6. For three-dimensional flow, it will be assumed that at each radius the flow mixes circumferentially to a uniform state. The radial character of the flow at the aftermixed state is therefore preserved. And the radial variation of the flow properties obtained in this manner can be used in the rotor design. The determination of the aftermixed state (station 3M) from survey measurements (station 3) for three-dimensional flow is discussed in the following paragraphs.

The aftermixed conditions are obtained by applying the conservation of mass, momentum, and energy equations to the control volume shown in figure 14. As discussed previously, it is assumed that the stream surfaces are circular. The control volume is chosen so that flow enters and leaves only through the annular sectors at stations 3 and 3M, respectively. The thickness of the control volume in the radial direction is assumed to be infinitesimal since this will permit the aftermixed conditions to be obtained as a function of radial position. In application of the conservation equations, it is assumed that viscous terms are negligible and that the pressure terms on the side faces of the control volume cancel because of symmetry.

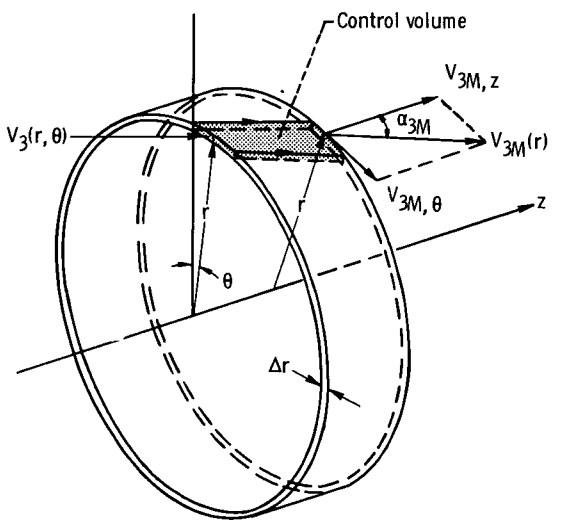

Figure 14. - Control volume for determination of aftermixed conditions (station 3M).

The conservation of mass requires that

$$\int_0^{\Theta} \rho_3(r, \theta) V_{3,z}(r, \theta) r \, d\theta = \rho_{3M}(r) V_{3M,z}(r) r\Theta \tag{B6}$$

The conservation of momentum in the axial direction gives

$$\int_0^{\Theta} \left[\rho_3(r, \theta) V_{3,z}^2(r, \theta) + g p_3(r, \theta)\right] r \, d\theta = \left[\rho_{3M}(r) V_{3M,z}^2(r) + g p_{3M}(r)\right] r\Theta \tag{B7}$$

Taking advantage of the circular geometry by determining the moment of the tangential forces gives

$$\int_0^{\Theta} \left[\rho_3(r, \theta) V_{3,z}(r, \theta) r V_{3,\theta}(r, \theta)\right] r \, d\theta = \left[\rho_{3M}(r) V_{3M,z}(r) r V_{3M,\theta}(r)\right] r\Theta \tag{B8}$$

where the tangential velocity $V_{3,\theta}(r, \theta)$ is given by

$$V_{3,\theta}(r, \theta) = V' \quad \cdots \quad r, \theta) \tag{B9}$$

It will be assumed that the total temperature $T_3'(r, \theta)$ at the measuring station is <u>not</u> constant. This assumption will permit the results to be used for both cooled and uncooled vanes. Conservation of energy therefore gives

$$\int_0^{\Theta} \rho_3(r, \theta) V_{3,z}(r, \theta) \left[C_p T_3(r, \theta) + \frac{V_3^2(r, \theta)}{2gJ}\right] r \, d\theta = \rho_{3M}(r) V_{3M,z}(r) \left[C_p T_{3M}(r) + \frac{V_{3M}^2(r)}{2gJ}\right] r\Theta \tag{B10}$$

The perfect-gas relation gives

$$\rho_{3M}(r) = \frac{p_{3M}(r)}{R T_{3M}(r)} \tag{B11}$$

We define

$$\overline{m}(r) = \int_0^{\Theta} \rho_3(r,\theta)V_{3,z}(r,\theta)\,d\theta = \rho_{3M}(r)V_{3M,z}(r)\Theta \tag{B12}$$

$$J_z(r) = \frac{\int_0^{\Theta}\left[\rho_3(r,\theta)V_{3,z}^2(r,\theta) + gp_3(r,\theta)\right]d\theta}{\int_0^{\Theta}\rho_3(r,\theta)V_{3,z}(r,\theta)\,d\theta} \tag{B13}$$

$$J_\theta(r) = \frac{\int_0^{\Theta}\rho_3(r,\theta)V_{3,z}(r,\theta)V_{3,\theta}(r,\theta)\,d\theta}{\int_0^{\Theta}\rho_3(r,\theta)V_{3,z}(r,\theta)\,d\theta} \tag{B14}$$

$$E(r) = \frac{\int_0^{\Theta}\rho_3(r,\theta)V_{3,z}(r,\theta)\left[C_pT_3(r,\theta) + \frac{V_3^2(r,\theta)}{2gJ}\right]d\theta}{\int_0^{\Theta}\rho_3(r,\theta)V_{3,z}(r,\theta)\,d\theta} \tag{B15}$$

Substituting these definitions into equations (B7), (B8), and (B10) results in

$$J_z(r) = V_{3M,z}(r) + \frac{gp_{3M}(r)}{\rho_{3M}(r)V_{3M,z}(r)} \tag{B16}$$

$$J_\theta(r) = V_{3M,\theta}(r) \tag{B17}$$

$$E(r) = C_pT_{3M}(r) + \frac{V_{3M}^2(r)}{2gJ} \tag{B18}$$

The functions $J_z(r)$, $J_\theta(r)$, and $E(r)$ are determined from the survey measurements at station 3 and are therefore known quantities. From equations (B11) and (B18),

$$\frac{p_{3M}(r)}{\rho_{3M}(r)} = RT_{3M}(r) = \frac{R}{C_p}\left[E(r) - \frac{V_{3M}^2(r)}{2gJ}\right] \tag{B19}$$

Since

$$V_{3M}^2(r) = V_{3M,z}^2(r) + V_{3M,\theta}^2(r) = V_{3M,z}^2(r) + J_\theta^2(r) \tag{B20}$$

equation (B19) becomes

$$\frac{p_{3M}(r)}{\rho_{3M}(r)} = \frac{R}{C_p}\left\{E(r) - \left[\frac{V_{3M,z}^2(r) + J_\theta^2(r)}{2gJ}\right]\right\} \tag{B21}$$

Substituting equation (B21) into equation (B16) and rearranging gives a quadratic equation for the aftermixed axial velocity $V_{3M,z}(r)$

$$\left(1 - \frac{R}{2C_pJ}\right)V_{3M,z}^2(r) - J_z(r)V_{3M,z}(r) + \frac{gR}{C_p}\left[E(r) - \frac{J_\theta^2(r)}{2gJ}\right] = 0 \tag{B22}$$

For a perfect gas with constant specific heats, R, C_p, and γ are related through the equation

$$\frac{R}{C_pJ} = \frac{\gamma - 1}{\gamma} \tag{B23}$$

Therefore, equation (B22) becomes, after substitution of equation (B23) and rearranging,

$$V_{3M,z}^2(r) - \frac{2\gamma}{\gamma + 1}J_z(r)V_{3M,z}(r) + \frac{\gamma - 1}{\gamma + 1}\left[2gJE(r) - J_\theta^2(r)\right] = 0 \tag{B24}$$

Solution of equation (B24) gives

$$V_{3M,z}(r) = \frac{\gamma}{\gamma+1} J_z(r) - \sqrt{\left[\frac{\gamma}{\gamma+1} J_z(r)\right]^2 - \frac{\gamma-1}{\gamma+1}\left[2gJE(r) - J_\theta^2(r)\right]} \tag{B25}$$

where the negative sign has been used for the usual case of subsonic axial velocities. The aftermixed velocity $V_{3M}(r)$ is found from equation (B20).

The aftermixed flow angle $\alpha_{3M}(r)$ is found from

$$\alpha_{3M}(r) = \tan^{-1}\left[\frac{V_{3M,\theta}(r)}{V_{3M,z}(r)}\right] = \tan^{-1}\left[\frac{J_\theta(r)}{V_{3M,z}(r)}\right] \tag{B26}$$

The aftermixed conditions of density $\rho_{3M}(r)$, static temperature $T_{3M}(r)$, and static pressure $p_{3M}(r)$ are found from equations (B12), (B18), and (B11), respectively. The aftermixed total pressure $p'_{3M}(r)$ and total temperature $T'_{3M}(r)$ are obtained from

$$\frac{p'_{3M}(r)}{p_{3M}(r)} = \left[1 + \frac{\gamma-1}{2} M_{3M}^2(r)\right]^{\frac{\gamma}{\gamma-1}} = \left[\frac{T'_{3M}(r)}{T_{3M}(r)}\right]^{\frac{\gamma}{\gamma-1}} \tag{B27}$$

where the aftermixed Mach number $M_{3M}(r)$ is given by

$$M_{3M}(r) = \frac{V_{3M}(r)}{\sqrt{\gamma g R T_{3M}(r)}} \tag{B28}$$

The aftermixed conditions have now been determined from the survey data ($\overline{m}(r)$, $J_z(r)$, $J_\theta(r)$, and $E(r)$). The derived relations are applicable to both cooled and uncooled vanes, since the total temperature $T'_3(r,\theta)$ has not been assumed constant. For uncooled vanes, it can be assumed that the total temperature T'_3 is constant and equal to the inlet total temperature T'_1. Therefore, $E(r) = C_p T'_1 = \text{Constant}$.

For uncooled vanes, the aftermixed efficiencies based on kinetic energy, similar to equations (B2) and (B3), are defined as

$$\bar{\eta}_{3M}(r) = \frac{V_{3M}^2(r)}{V_{3M,\,id}^2(r)} \tag{B29}$$

$$\bar{\bar{\eta}}_{3M} = \frac{\int_{r_i}^{r_o} \rho_{3M}(r) V_{3M,\,z}(r) V_{3M}^2(r) r\, dr}{\int_{r_i}^{r_o} \rho_{3M}(r) V_{3M,\,z}(r) V_{3M,\,id}^2(r) r\, dr} \tag{B30}$$

where

$$V_{3M,\,id}(r) = \sqrt{\left(\frac{2\gamma}{\gamma - 1}\right) g R T_1' \left\{1 - \left[\frac{p_{3M}(r)}{p_1'}\right]^{\frac{\gamma-1}{\gamma}}\right\}} \tag{B31}$$

In addition, a total-pressure-loss coefficient is defined as

$$\bar{\omega}_{3M}(r) = \frac{p_1' - p_{3M}'(r)}{p_1' - p_{3M}(r)} \tag{B32}$$

For completeness, the definitions of efficiency used for cooled vanes will be given. The thermodynamic efficiency and the primary efficiency are in general use for cooled vanes. The thermodynamic efficiency is defined as the ratio of the actual vane kinetic energy to the sum of the ideal kinetic energies of both the primary and coolant flows. The thermodynamic aftermixed efficiencies are given by

$$\bar{\eta}_{3M,\,T}(r) = \frac{V_{3M}^2(r)}{y_p(r)\left[V_{3M,\,id}^2(r)\right]_p + y_c(r)\left[V_{3M,\,id}^2(r)\right]_c} \tag{B33}$$

and

$$\bar{\bar{\eta}}_{3M,T} = \frac{\int_{r_i}^{r_o} \left[\rho_{3M}(r) V_{3M,z}(r) V_{3M}^2(r)\right] r\, dr}{\int_{r_i}^{r_o} \rho_{3M}(r) V_{3M,z}(r) \left\{ y_p(r) \left[V_{3M,id}^2(r)\right]_p + y_c(r) \left[V_{3M,id}^2(r)\right]_c \right\} r\, dr} \tag{B34}$$

where the ideal velocities of the primary $\left[V_{3M,id}(r)\right]_p$ and coolant $\left[V_{3M,id}(r)\right]_c$ are given by

$$\left[V_{3M,id}(r)\right]_p = \sqrt{\frac{2\gamma}{\gamma - 1} gRT_1' \left\{ 1 - \left[\frac{p_{3M}(r)}{p_1'}\right]^{\frac{\gamma-1}{\gamma}} \right\}} \tag{B35}$$

$$\left[V_{3M,id}(r)\right]_c = \sqrt{\frac{2\gamma}{\gamma - 1} gRT_c' \left\{ 1 - \left[\frac{p_{3M}(r)}{p_c'}\right]^{\frac{\gamma-1}{\gamma}} \right\}} \tag{B36}$$

The fraction of coolant flow to total flow $y_c(r)$ and the fraction of primary flow to total flow $y_p(r)$ are given by

$$y_c(r) = \frac{\bar{\bar{m}}_c(r)}{\bar{\bar{m}}(r)} = 1 - y_p(r) \tag{B37}$$

The variation of coolant flow $\bar{\bar{m}}_c(r)$ with radius is not easily measured and can either be estimated theoretically or be assumed to vary with radius in a similar manner as the total flow $\bar{\bar{m}}(r)$. In this situation, $y_c(r)$ is constant with radius and is given by the equation

$$\bar{y}_c = \frac{\bar{\bar{m}}_c}{\bar{\bar{m}}} = \text{Constant} \tag{B38}$$

where the total flow $\overline{\overline{m}}$ is

$$\overline{\overline{m}} = \int_{r_h}^{r_t} \int_0^{\Theta} \rho_3(r,\theta) V_{3,z}(r,\theta) r \, d\theta \, dr = \int_{r_h}^{r_t} \overline{m}(r) r \, dr \tag{B39}$$

The primary efficiency is defined as the ratio of the actual vane kinetic energy to the ideal kinetic energy of the primary flow only. The primary aftermixed efficiencies are given by

$$\overline{\eta}_{3M,p}(r) = \frac{V_{3M}^2(r)}{y_p(r)\left[V_{3M,id}^2(r)\right]_p} \tag{B40}$$

$$\overline{\overline{\eta}}_{3M,p} = \frac{\int_{r_i}^{r_o} \left[\rho_{3M}(r) V_{3M,z}(r) V_{3M}^2(r)\right] r \, dr}{\int_{r_i}^{r_o} \left\{y_p(r) \rho_{3M}(r) V_{3M,z}(r) \left[V_{3M,id}^2(r)\right]_p\right\} r \, dr} \tag{B41}$$

For zero coolant flow ($y_c(r) = 0$), the thermodynamic efficiencies (eqs. (B33) and (B34)) are equal to the primary efficiencies (eqs. (B40) and (B41)) and reduce to the relations given for the uncooled vane efficiencies in equations (B29) and (B30).

The aftermixed equations derived herein ((B25) to (B28)) are also applicable to two-dimensional flow. This is accomplished by making the identification

$$\left.\begin{aligned} r \, d\theta &\rightarrow du \\ r\Theta &\rightarrow s \end{aligned}\right\} \tag{B42}$$

where u is the coordinate in the tangential direction for two-dimensional flow and s is the vane spacing in meters (ft). Of course, overall aftermixed efficiencies have no meaning in this special case.

REFERENCES

1. Gladden, Herbert J.; Dengler, Robert P.; Evans, David G.; and Hippensteele, Steven A.: Aerodynamic Investigation of Four-Vane Cascade Designed for Turbine Cooling Studies. NASA TM X-1954, 1970.

2. Stabe, Roy G.; and Dengler, Robert P.: Experimental Investigation of Aerodynamic Performance of Cooled Turbine Vanes at Gas- to Coolant-Temperature Ratios up to 2.75. NASA TM X-2733, 1973.

3. Katsanis, Theodore: FORTRAN Program for Quasi-Three-Dimensional Calculation of Surface Velocities and Choking Flow for Turbomachine Blade Rows. NASA TN D-6177, 1971.

4. Katsanis, Theodore: FORTRAN Program for Calculating Transonic Velocities on a Blade-to-Blade Stream Surface of a Turbomachine. NASA TN D-5427, 1969.

5. Rohlik, Harold E.; Kofskey, Milton G.; Allen, Hubert W.; and Herzig, Howard Z.: Secondary Flows and Boundary-Layer Accumulations in Turbine Nozzles. NACA Rep. 1168, 1954.

6. Stewart, Warner L.: Analysis of Two-Dimensional Compressible-Flow Loss Characteristics Downstream of Turbomachine Blade Rows in Terms of Basic Boundary-Layer Characteristics. NACA TN 3515, 1955.

NATIONAL AERONAUTICS AND SPACE ADMINISTRATION
WASHINGTON, D.C. 20546

OFFICIAL BUSINESS
PENALTY FOR PRIVATE USE $300

SPECIAL FOURTH-CLASS RATE
BOOK

POSTAGE AND FEES PAID
NATIONAL AERONAUTICS AND
SPACE ADMINISTRATION
451

U.S.MAIL

POSTMASTER: If Undeliverable (Section 158 Postal Manual) Do Not Return

"The aeronautical and space activities of the United States shall be conducted so as to contribute . . . to the expansion of human knowledge of phenomena in the atmosphere and space. The Administration shall provide for the widest practicable and appropriate dissemination of information concerning its activities and the results thereof."

—NATIONAL AERONAUTICS AND SPACE ACT OF 1958

NASA SCIENTIFIC AND TECHNICAL PUBLICATIONS

TECHNICAL REPORTS: Scientific and technical information considered important, complete, and a lasting contribution to existing knowledge.

TECHNICAL NOTES: Information less broad in scope but nevertheless of importance as a contribution to existing knowledge.

TECHNICAL MEMORANDUMS: Information receiving limited distribution because of preliminary data, security classification, or other reasons. Also includes conference proceedings with either limited or unlimited distribution.

CONTRACTOR REPORTS: Scientific and technical information generated under a NASA contract or grant and considered an important contribution to existing knowledge.

TECHNICAL TRANSLATIONS: Information published in a foreign language considered to merit NASA distribution in English.

SPECIAL PUBLICATIONS: Information derived from or of value to NASA activities. Publications include final reports of major projects, monographs, data compilations, handbooks, sourcebooks, and special bibliographies.

TECHNOLOGY UTILIZATION PUBLICATIONS: Information on technology used by NASA that may be of particular interest in commercial and other non-aerospace applications. Publications include Tech Briefs, Technology Utilization Reports and Technology Surveys.

Details on the availability of these publications may be obtained from:

SCIENTIFIC AND TECHNICAL INFORMATION OFFICE

NATIONAL AERONAUTICS AND SPACE ADMINISTRATION

Washington, D.C. 20546